01 May 2009

Multimodal Solution for a Waveguide Radiating into Multilayered Structures -- Dielectric Properties and Thickness Evaluation

Mohammad Tayeb Ahmad Ghasr
Missouri University of Science and Technology, mtg7w6@mst.edu

Devin L. Simms

R. Zoughi
Missouri University of Science and Technology, zoughi@mst.edu

Recommended Citation

M. T. Ghasr et al., "Multimodal Solution for a Waveguide Radiating into Multilayered Structures -- Dielectric Properties and Thickness Evaluation," *IEEE Transactions on Instrumentation and Measurement*, vol. 58, no. 5, pp. 1505-1513, Institute of Electrical and Electronics Engineers (IEEE), May 2009.
The definitive version is available at https://doi.org/10.1109/TIM.2008.2009133

Multimodal Solution for a Waveguide Radiating Into Multilayered Structures—Dielectric Property and Thickness Evaluation

M. T. Ghasr, *Student Member, IEEE*, Devin Simms, and R. Zoughi, *Fellow, IEEE*

***Abstract*—Open-ended rectangular waveguides are widely used for microwave and millimeter-wave nondestructive testing (NDT) applications, such as detecting disbond and delamination in multilayered composite structures, thickness evaluation of dielectric sheets and coatings on metal substrates, etc. When inspecting a complex multilayered composite structure that is made of generally lossy dielectric layers with arbitrary thicknesses and backing, the dielectric properties of a particular layer may be of particular interest (e.g., radome inspection). The same is also true when one is interested in the thickness, or, more importantly, thickness variation, of a particular layer within such complex structures. An essential tool for closely estimating the complex permittivity and/or thickness is an accurate forward electromagnetic model for simulating the reflection coefficient at the aperture of the probing open-ended waveguide. To this end, this paper provides a full-wave accurate forward model for calculating the reflection coefficient from a generally lossy multilayered composite structure possessing an arbitrary number of layers and respective thicknesses while accounting for the influence of higher order modes. This model is subsequently validated through comparisons with a commercial numerical tool and actual measurements. Furthermore, a measurement model is provided, which results in an iterative inverse technique for estimating the complex permittivity and thickness of a dielectric layer. Subsequently, this technique is applied to the measured reflection coefficients of several structures. To evaluate the accuracy of this technique, an analysis on its sensitivity to various sources of errors, and, most importantly, the effect of a finite flange size, is also demonstrated by using the simulated data. Finally, the potential of this model to accurately estimate the thickness of an individual layer, which represents a thin disbond, in a multilayered composite structure is presented.**

***Index Terms*—Complex permittivity, higher order modes, open-ended waveguide, stratified dielectric medium, thickness.**

I. Introduction

OPEN-ENDED rectangular waveguides are the most widely used probes for near-field microwave and millimeter-wave nondestructive testing (NDT) applications, such as dielectric property measurement of materials, thickness measurement of dielectric slabs, surface-breaking crack detection in metals, and porosity level estimation in ceramics and polymers, to name a few [1]. When operating in the near field of such a probe, the spatial resolution is a function of the probe dimensions, and hence, obtaining high-resolution images is readily possible at microwave and millimeter-wave frequencies since the probe dimensions are relatively small. Hence, these NDT methods compete very well with the other NDT methods [1], [2]. In addition, when concerned with multilayered composite structures, a thickness variation detection can be conducted with micrometer-range accuracy at relatively low microwave frequencies [1]–[5]. Microwave NDT also has the potential of providing information about the electrical properties of the dielectric structures. This is particularly important for inspecting structures such as radomes since the electrical properties of each layer in the structure directly affect whether a radome is transparent to electromagnetic radiation [6]. Dielectric property measurement using open-ended rectangular waveguides has received significant attention from both the modeling and experimental points of view. These works have primarily been focused on the inspection of multilayered structures or infinite half spaces [5], [7]–[12]. An issue of concern when evaluating the properties (thickness or dielectric) of a particular layer in a multilayered composite is that, if the effect of that layer on the overall reflection coefficient becomes small, then any small modeling or measurement error may result in a substantial error in the estimation of the desired layer properties. In such cases, the error is commonly attributed to the fact that the influence of higher order modes is ignored, and only the influence of the dominant mode is taken into account. Subsequently, this may result in slight or significant errors when the model is used in an inverse manner for the purpose of retrieving the complex permittivity or thickness of a layer from the measured reflection coefficient. Some of the prior studies have utilized variational methods, which result in an approximate solution [5], and some utilize more rigorous formulations while accounting for the effect of higher order modes [7]–[12]. Although many of these methods can be used to obtain the complex permittivity of a material, the sources of errors such as the choice of higher order modes, design of experimental setup, and the influence of noise or measurement uncertainty have not fully been studied. For example, no study has shown the contribution of higher order modes as a function of the various features of a multilayered structure such as layer thickness, dielectric profile, and whether the composite is backed by a dielectric infinite half space or a conducting plate. Furthermore, no study has shown the accuracy of the open-ended waveguide technique for measuring the relative complex

Manuscript received June 26, 2008; revised August 29, 2008. First published January 9, 2009; current version published April 7, 2009. The Associate Editor coordinating the review process for this paper was Dr. Matteo Pastorino.

The authors are with the Applied Microwave Nondestructive Testing Laboratory, Electrical and Computer Engineering Department, Missouri University of Science and Technology, Rolla, MO 65409 USA (e-mail: mtg7w6@mst.edu; dlsfff@mst.edu; zoughir@mst.edu).

Color versions of one or more of the figures in this paper are available online at http://ieeexplore.ieee.org.

Digital Object Identifier 10.1109/TIM.2008.2009133

permittivity and thickness of the thin layers, and an analysis of the sources of errors when considering thin dielectric layers such as a disbond. As will be shown in this paper, the effect of higher order modes is much more significant when analyzing a multilayered composite structure than when analyzing an infinite half space of a material. The size of the flange is another issue not fully addressed in previous investigations. Many studies, for example, [10] and [11], either considered a very large flange or used the waveguide radiation pattern to determine the proper size of the flange.

This paper is an extension of the preliminary work reported in [13], which gives an exact formulation for the reflection coefficient at the aperture of an open-ended rectangular waveguide irradiating a multilayered dielectric structure. This formulation accounts for the contribution of transverse electric (TE) and transverse magnetic (TM) higher order modes. Furthermore, an analysis of the effect of higher order modes as a function of parameters such as layer thickness and complex permittivity and the number of higher order modes required for convergence was presented in [13] followed by an example of estimating the complex permittivity of a lossy rubber sheet. In this paper, the formulation is validated by using the measured results obtained from a multilayered structure consisting of lossy rubber and low-loss acrylic sheets. Subsequently, the measured results are used to estimate the complex permittivity of the two dielectric sheets. Moreover, a model for the measured reflection coefficient is provided, which leads to an optimum cost function that is used in the inverse technique for estimating the desired complex permittivity and thickness of a layer. Subsequently, the performance of this technique in estimating the complex permittivity of a sheet of dielectric within a multilayered structure is evaluated. Furthermore, a detailed examination of the effect of using a finite flange is presented and ultimately validated by measuring the complex permittivity and thickness of rubber sheets with different thicknesses. Finally, a multilayered composite structure with thin dielectric layers representing disbonds and/or adhesive layers is examined, and the thickness of these thin layers are determined by using the simulated and measured reflection coefficient data.

II. Formulation

In this paper, the reflection coefficient seen by an open-ended waveguide radiating into a multilayered dielectric structure is formulated in a similar fashion as [9] and [12]. Yoshitomi and Sharobim [9] considered an open-ended waveguide aperture terminated in a lossy flange and radiating into free space for the purpose of examining the flange influence on the radiation pattern, whereas Bois *et al.* [12] expanded these formulations for an accurate extraction of the complex permittivity of a generally lossy infinite half space of a dielectric material. This paper extends this formulation to a general case of a multilayered dielectric medium possessing any number of layers and backed by an infinite half space or a conductor for the purpose of an accurate extraction of the complex permittivity or the thickness of any arbitrary layer. Fig. 1 shows a schematic of an open-ended waveguide aperture radiating into a multilayered structure. The waveguide aperture has a broad dimension of $2a$ and a narrow dimension of $2b$, cut into of an infinite conducting

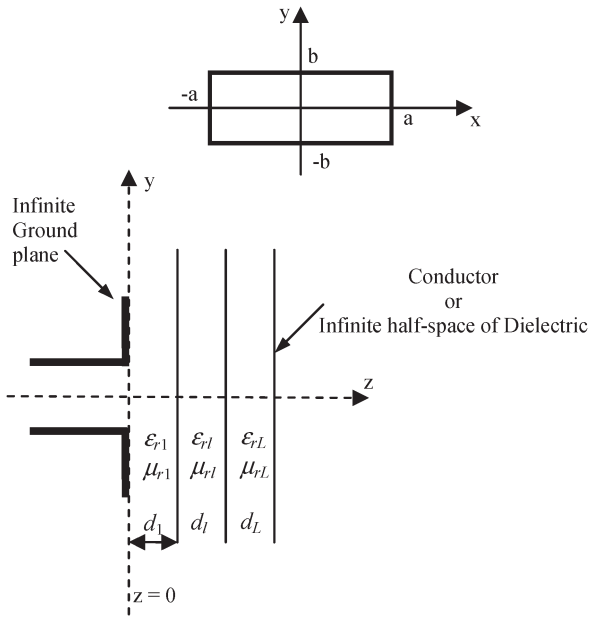

Fig. 1. Geometry of the problem.

ground plane or flange, and radiating into a multilayered dielectric structure backed by a conductor or an infinite half space of a dielectric material. Each layer is defined by its relative (to free space) complex permittivity ($\varepsilon_r = \varepsilon_r' - j\varepsilon_r''$) and relative complex permeability ($\mu_r = \mu_r' - j\mu_r''$) as well as its thickness d. The imaginary parts of the relative complex permittivity and permeability represent the attenuation of the wave in the material and are referred to as *loss factor* henceforth.

The electric and magnetic fields in all the regions may be derived from the Hertzian vectors. For the incident field inside the waveguide, a magnetic Hertzian vector with the dominant TE_{10} mode distribution is used. On the other hand, the reflected waves are represented by the electric and magnetic Hertzian vectors, which represent a summation of *all* the possible TM and TE waveguide modes. The definition for these Hertzian vectors may be found in [9] and [12] and not repeated here.

In [9] and [12], the Hertzian vectors (outside the waveguide) were defined for the case of an infinite half space, where only a forward traveling wave exists. In a multilayered dielectric structure, both forward and backward traveling waves exist. Consequently, the definition of the electric and magnetic Hertzian vectors is changed accordingly as

$$\hat{a}_z \cdot \prod_l^e (x,y,z) = \frac{1}{4\pi^2 k_l^2} \int_{-\infty}^{\infty}\int_{-\infty}^{\infty} \left[A_l^{e+}(\xi,\eta)e^{-j\zeta z} + A_l^{e-}(\xi,\eta)e^{j\zeta z}\right] \times e^{-j(\xi x+\eta y)} d\xi d\eta \quad (1)$$

$$\hat{a}_z \cdot \prod_l^h (x,y,z) = \frac{1}{4\pi^2 k_l^2 Z_l} \int_{-\infty}^{\infty}\int_{-\infty}^{\infty} \left[A_l^{h+}(\xi,\eta)e^{-j\zeta z} + A_l^{h-}(\xi,\eta)e^{j\zeta z}\right] \times e^{-j(\xi x+\eta y)} d\xi d\eta \quad (2)$$

where $k=\omega\sqrt{\varepsilon.\mu}$, $Z=\sqrt{\mu/\varepsilon}$, $\zeta=\sqrt{k^2-\xi^2-\eta^2}$, and $A^{e,h}(\xi,\eta)$ are the spectral domain wave functions representing the radiated electromagnetic fields from the waveguide. These functions are unknown and are determined subject to specific boundary conditions. Since the discontinuities are along the z-direction, both forward and backward propagating waves, which are denoted by $+$ and $-$ superscripts, respectively, are present in each layer. Furthermore, the subscript $l=1,2,\ldots,L$ denotes the layer number. The expressions for converting the Hertzian vectors into electric and magnetic fields and the Fourier relationships to transform the field between the spatial and spectral domains may be found in [9] and [12] and will not be repeated here.

The reflection coefficient at the open-ended waveguide is obtained by matching the boundary conditions at all the interfaces and begins at the last layer ($z=z_L$). For a conductor-backed case, the tangential electric field (at the conductor boundary) vanishes, which results in the total reflection

$$A_L^{e-}=A_L^{e+}e^{-2j\zeta_L z_L},\quad A_L^{h-}=-A_L^{h+}e^{-2j\zeta_L z_L}. \tag{3}$$

On the other hand, for an infinite half-space case, the backward traveling wave is zero since there is no mechanism for reflections, which results in

$$A_L^{e-}=0,\quad A_L^{h-}=0. \tag{4}$$

Matching the boundary conditions at the intermediate layers results in the following relationships between the forward and backward traveling waves:

$$\frac{A_{l-1}^{e-}}{A_{l-1}^{e+}}=e^{-2j\zeta_{l-1}z_{l-1}}\times\frac{C_l^e e^{2j\zeta_l z_{l-1}}(1+B_l^e)-e^{2j\zeta_l z_l}(1-B_l^e)}{-C_l^e e^{2j\zeta_l z_{l-1}}(1-B_l^e)+e^{2j\zeta_l z_l}(1+B_l^e)} \tag{5}$$

where

$$B_l^e=\frac{Z_{l-1}k_l\zeta_{l-1}}{Z_l k_{l-1}\zeta_l} \tag{6}$$

$$C_{l-1}^e=\frac{C_l^e e^{-2j\zeta_l d_l}(1+B_l^e)-(1-B_l^e)}{-C_l^e e^{-2j\zeta_l d_l}(1-B_l^e)+(1+B_l^e)}. \tag{7}$$

Similar expressions are obtained for the magnetic field components

$$B_l^h=\frac{Z_l k_l\zeta_{l-1}}{Z_{l-1}k_{l-1}\zeta_l} \tag{8}$$

$$C_{l-1}^h=\frac{C_l^h e^{-2j\zeta_l d_l}\left(1+B_l^h\right)-\left(1-B_l^h\right)}{-C_l^h e^{-2j\zeta_l d_l}\left(1-B_l^h\right)+\left(1+B_l^h\right)}. \tag{9}$$

The $C^{e,h}$ coefficients are iteratively obtained starting from the last layer, where $C_L^e=-C_L^h=1$ for a conductor-backed case, and $C_L^h=C_L^e=0$ for an infinite half-space case.

The boundary conditions at the waveguide aperture ($z=0$) dictate the continuity of the total electric and magnetic fields as

$$\overline{E}_{x,y}^1=\begin{cases}\overline{E}_{x,y}^{wg}, & |x|\le a,|y|\le b\\ 0, & \text{elsewhere}\end{cases} \tag{10}$$

$$\overline{H}_{x,y}^1=\overline{H}_{x,y}^{wg},\qquad |x|\le a,|y|\le b \tag{11}$$

where the superscript wg denotes the total fields in the waveguide, and the superscript 1 refers to the total fields in the first layer. Applying these boundary conditions and utilizing the orthogonal properties of the modes in the waveguide in a very similar fashion to [9] and [12] results in the following two linear systems of equations:

$$\begin{aligned}&\sum_{m,n=1}^{\infty}\left[a_m I_1(m,n,p,q)+b_n I_2(m,n,p,q)\right]k_{mn}A_{mn}^e\\&+\sum_{\substack{m,n=0\\ m=n\neq 0}}^{\infty}\left[b_n I_1(m,n,p,q)-a_m I_2(m,n,p,q)\right]k_0 A_{mn}^h\\&+ab\left[A_{pq}^e k_0 b_q-A_{pq}^h k_{pq}a_p(1+\delta_{0q})\right]\frac{Z_1}{Z_0}\\&\quad=\left[k_0 a_1 I_2(1,0,p,q)-2k_{10}a_1 ab\frac{Z_1}{Z_0}\delta_{1p}\delta_{0q}\right]A^i\end{aligned} \tag{12}$$

for $p=1,2,3,\ldots$, $q=0,1,2,3,\ldots$, and

$$\begin{aligned}&\sum_{m,n=1}^{\infty}\left[a_m I_3(m,n,p,q)+b_n I_4(m,n,p,q)\right]k_{mn}A_{mn}^e\\&+\sum_{\substack{m,n=0\\ m=n\neq 0}}^{\infty}\left[b_n I_3(m,n,p,q)-a_m I_4(m,n,p,q)\right]k_0 A_{mn}^h\\&+ab\left[A_{pq}^e k_0 a_p+A_{pq}^h k_{pq}b_q(1+\delta_{0p})\right]\frac{Z_1}{Z_0}\\&\quad=k_0 a_1 I_4(1,0,p,q)A^i\end{aligned} \tag{13}$$

for $p=0,1,2,3,\ldots$, $q=1,2,3,\ldots$, where, m, n, p, and q are the integers that represent the mode numbers. In the foregoing equations, A^i is the complex amplitude of the incident TE_{10} field, whereas A_{mn}^e and A_{mn}^h are the coefficients of the reflected and/or generated TM and TE modes at the waveguide aperture. The summations and these coefficients represent the mapping of the aperture electromagnetic fields on the waveguide modes. These modes only exist at the aperture of the waveguide, and only the dominant mode reflection coefficient A_{10}^h is measured in practice. The rest of the variables are defined as $a_m=m\pi/2a$, $b_n=n\pi/2b$, $k_{mn}=\sqrt{k_0^2-a_m^2-b_n^2}$, and δ_{pq} is the Kronecker delta, and the integrals $I_{1,2,3,4}$ are

$$\begin{aligned}&I_1(m,n,p,q)\\&=\frac{1}{4\pi^2}\int_{-\infty}^{\infty}\int_{-\infty}^{\infty}V_1 C_m^a(-\xi)S_n^b(-\eta)S_p^a(\xi)C_q^b(\eta)d\xi d\eta\end{aligned} \tag{14}$$

$$\begin{aligned}&I_2(m,n,p,q)\\&=\frac{1}{4\pi^2}\int_{-\infty}^{\infty}\int_{-\infty}^{\infty}V_2 S_m^a(-\xi)C_n^b(-\eta)S_p^a(\xi)C_q^b(\eta)d\xi d\eta\end{aligned} \tag{15}$$

$$\begin{aligned}&I_3(m,n,p,q)\\&=\frac{1}{4\pi^2}\int_{-\infty}^{\infty}\int_{-\infty}^{\infty}V_3 C_m^a(-\xi)S_n^b(-\eta)C_p^a(\xi)S_q^b(\eta)d\xi d\eta\end{aligned} \tag{16}$$

$$\begin{aligned}&I_4(m,n,p,q)\\&=\frac{1}{4\pi^2}\int_{-\infty}^{\infty}\int_{-\infty}^{\infty}V_1 S_m^a(-\xi)C_n^b(-\eta)C_p^a(\xi)S_q^b(\eta)d\xi d\eta.\end{aligned} \tag{17}$$

The C's and S's in the preceding integrals are the cosine and sine integrals as defined in [12]. The variables $V_{1,2,3}$ represent the spatial spectral domain field distribution at the aperture of the waveguide containing information about the properties of the multilayered dielectric structure, which are defined as

$$V_1 = \frac{k_1^2\eta\xi - \zeta_1^2\eta\xi D_1^h D_1^e}{k_1(\xi^2+\eta^2)\zeta_1 D_1^e} \tag{18}$$

$$V_2 = \frac{k_1^2\eta^2 + \zeta_1^2\xi^2 D_1^h D_1^e}{k_1(\xi^2+\eta^2)\zeta_1 D_1^e} \tag{19}$$

$$V_3 = \frac{k_1^2\xi^2 + \zeta_1^2\eta^2 D_1^h D_1^e}{k_1(\xi^2+\eta^2)\zeta_1 D_1^e} \tag{20}$$

$$D_1^h = \frac{1 - C_1^h e^{-2j\zeta_1 d_1}}{1 + C_1^h e^{-2j\zeta_1 d_1}} \tag{21}$$

$$D_1^e = \frac{1 - C_1^e e^{-2j\zeta_1 d_1}}{1 + C_1^e e^{-2j\zeta_1 d_1}}. \tag{22}$$

The integrals in (14)–(17) may become singular, particularly when the *total* loss (associated with the complex permittivity of the layers) is relatively small. When numerically evaluating these integrals, it is advantageous to transform them to polar coordinates, as reported in [9]. However, unlike the cases investigated in [9] and [12], where the structure is always an infinite half space, and the singularity location is known and can analytically be extracted, in a multilayered structure, the singularity of the integrals depends on the profile of the structure. Therefore, it is not possible to analytically extract the singularities, and the integration must be performed and evaluated on a contour around the singular points. Furthermore, a conversion test must be performed prior to obtaining the final and acceptable solution.

III. Analysis

To verify and validate the formulation, the complex reflection coefficient ($\Gamma = |\Gamma| e^{\phi_\Gamma}$) seen by an X-band (8.2–12.4 GHz) waveguide radiating into free space was compared to the results obtained by using computer simulation technology–microwave studio (CST-MS) [14], which employs a 3-D electromagnetic simulation. The results, which are similar to the previously published data in [12], are shown in Fig. 2 in polar format. These results show that while there is a major advantage in including the higher order modes in the solution, their contribution becomes minimal beyond the first few modes. In fact, with only six modes, it is possible to determine an accurate solution, as also reported in [12]. Consequently, from now on, all of the solutions that include higher order modes will only utilize six modes.

In [12], it was shown that the error in the TE_{10} reflection coefficient due to the exclusion of higher order modes decreases as the permittivity and loss factor increase. However, this is only true when the waveguide is radiating into an infinite half space of a dielectric. When considering a finite dielectric slab (i.e., sheet) or a multilayered structure, the thickness of the dielectric layers has an effect on the contribution of the higher order modes as well. To investigate this phenomenon, simulations were performed for a slab of rubber with a relative complex permittivity of ($\varepsilon_r = 7.3 - j\ 0.3$) and a slab of acrylic

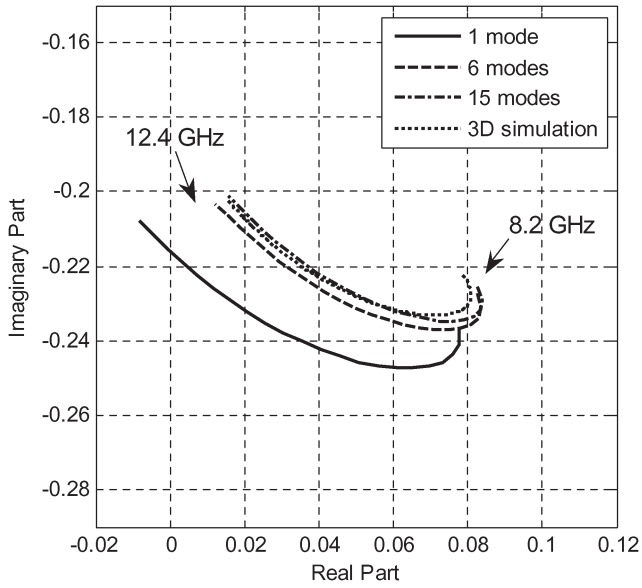

Fig. 2. Reflection coefficient seen by an X-band open-ended waveguide radiating into free space. The effect of higher order modes over the frequency band of 8.2–12.4 GHz (X-band).

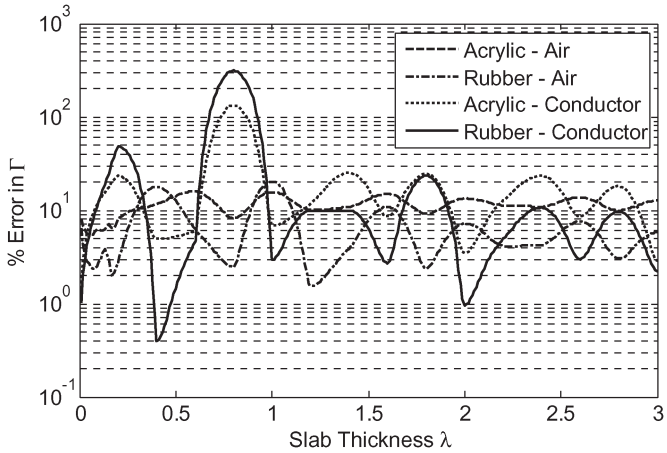

Fig. 3. Percent error in reflection coefficient calculation due to the exclusion of higher order modes versus normalized slab thickness.

with a relative complex permittivity of ($\varepsilon_r = 2.6 - j\ 0.01$). The reflection coefficient considering the higher order modes ($\Gamma_{w/\_HOM}$) and the reflection coefficient without considering the higher order modes (Γ_{w/o_HOM}) are simulated for each material with varying thickness. The percent error is defined as the Euclidean distance between these two simulated reflection coefficients and normalized to $\Gamma_{w/\_HOM}$. Two cases of conductor backed and an infinite half space of air backing were simulated for each slab. Fig. 3 shows the percentage error in terms of slab thickness (normalized to the wavelength in the dielectric slab). The results show that, for the case of an infinite half space of air, as the thickness of the slab increases (moving toward infinite half space), the materials with higher relative permittivity and loss factor (i.e., rubber) produce less significant higher order modes compared to the materials with low relative permittivity and loss factor (i.e., acrylic). These results are in agreement with the results reported in [12]. Conversely, when the thickness of the slab decreases, depending on the absolute value of the thickness, the opposite may occur, and

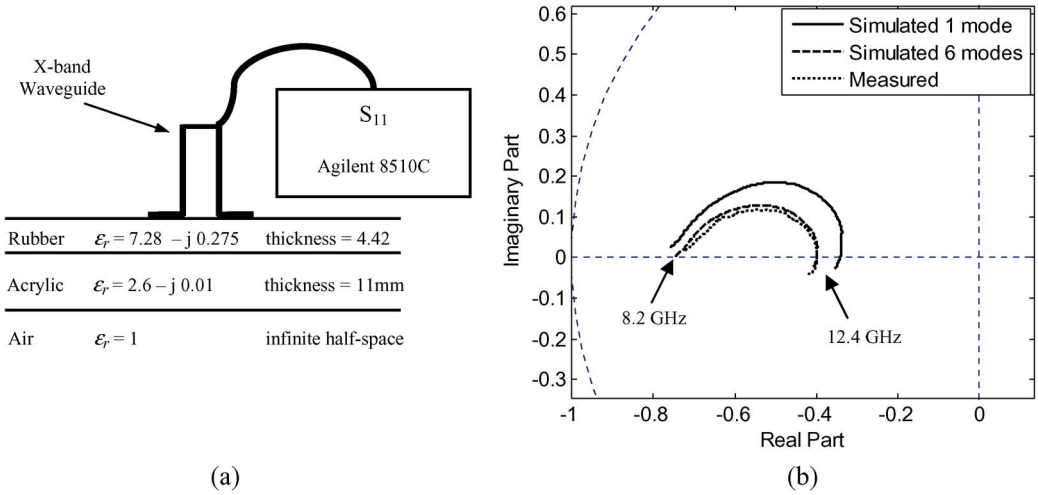

Fig. 4. Effect of higher order modes in the presence of a thin lossy material. (a) Measurement setup. (b) Measurement versus simulation results.

the contribution of higher order modes become more significant for high relative permittivity materials. This is attributed to the strong multiple reflections in a slab with a finite thickness. Furthermore, this effect becomes more prominent when the slab is backed by a conductor, as shown in Fig. 3. Fig. 4 shows a comparison between the measured results and the corresponding simulations for a three-layer structure made of rubber, acrylic, and an infinite half space of air backing [Fig. 4(a)]. The measurement was performed by using an Agilent 8510C vector network analyzer (VNA) with an X-band open-ended rectangular waveguide (with a standard flange). The results in Fig. 4(b) are shown in polar format. As expected (given the findings in Fig. 3), the presence of a thin lossy rubber at the opening of the waveguide and the multiple reflections in the structure increase the influence of higher order modes on the reflection coefficient. Furthermore, the effect of higher order modes is more prominent at the higher end of the frequency band, consistent with the results reported in [12].

IV. Inverse Problem

Consider a general inverse problem where the goal is to estimate or retrieve one of the physical or electrical properties of at least one layer in a multilayered composite structure. These unknown properties may be any one of the parameters from the set of $\{d_l, \varepsilon_{rl}, \text{and } \mu_{rl}\}$, where $l = 1, 2, \ldots, L$ is the layer number. Since the aforementioned forward model is noninvertible in a straightforward or direct fashion, iterative search algorithms are used to retrieve a desired unknown parameter. To reach an acceptable solution, all of the search algorithms require an optimum cost function that needs to be minimized. The measured complex reflection coefficient (Γ_m), which is a function of the operating frequency and the properties of the irradiated multilayered structure, namely, electromagnetic properties (ε_r and μ_r) and thicknesses (d), is described by

$$\Gamma_m(f_i, d, \varepsilon_r, \mu_r) = \Gamma_a(f_i, d, \varepsilon_r, \mu_r) + \gamma_i \tag{23}$$

where Γ_a is the actual reflection coefficient under ideal conditions (e.g., simulated), and γ_i represents the frequency-dependent measurement uncertainty. This uncertainty is a complex quantity that represents the collective error (or noise) in the measurements, which may be due to measurement system noise, modeling errors due to a finite-sized flange, errors in known or measured electrical or dimensional properties, etc. Hereon, γ_i, which is referred to as *noise*, is assumed to have a zero-mean Gaussian distribution with a variance of N_o (N_o is the total power in the noise). The Gaussian assumption, which is based on having several independent sources of uncertainties, is supported by the central limit theorem. Furthermore, it is a common practice to average the multiple measurements taken over time and space, which gives more credence to the aforementioned reasoning of the central limit theorem. Consequently, the optimum solution for the inverse problem is the solution that minimizes the cost function $|\Gamma_m - \Gamma_a|^2$ [3].

Since the forward model (Section II) is computationally intensive, fast converging algorithms are highly preferred when performing the iterative inverse parameter extraction. Sequential quadratic programming (SQP) has shown to outperform other search methods when considering its efficiency and accuracy. However, like other gradient search methods, it suffers from the possible convergence to the local minima [15], [16]. This problem is more significant in a multilayered structure due to the multiple reflections that make the measured reflection coefficient unpredictable and cause the cost function to have multiple local minima. The multiple local minima make the solution highly dependent on the choice of the initial guess value. Performing a multiple parallel search, as suggested in [15], alleviates this problem by searching for all the minima and eventually finding the global minima that lead to the optimum solution. This method, although effective in eliminating the convergence to the local minima, increases the search time. The solution proposed here is divided into two steps. In the first step, the diversity of the measurement over the frequency band is utilized. For this purpose, the cost function F is modified as

$$F = \frac{1}{N_f} \sum_{i=1}^{N_f} |\Gamma_m(f_i) - \Gamma_a(f_i)|^2 \tag{24}$$

TABLE I
ESTIMATING/RETRIEVING THE COMPLEX PERMITTIVITIES OF RUBBER AND ACRYLIC SHEETS

Unknown Material	Thickness	Loaded waveguide technique	This Study	
	(mm)	Actual ε_r	Including HOM	Excluding HOM
Rubber	4.42	7.28 – j 0.275	7.32 – j 0.25	7.45 – j 1.03
Acrylic	11	2.61 – j 0.012	2.58 – j 0.00	2.90 – j 0.079

where f_i's $(i = 1, 2, \ldots, N_f)$ are the discrete frequencies within the waveguide band. This cost function significantly reduces the number of local minima. Using this cost function and the fact that the relative complex permittivity dispersion of most materials within a narrow band of frequencies (such as the X-band used here) is usually small, SQP estimates an average solution for the desired material property. If the average solution is acceptable, then the process may be terminated at that point. Otherwise, a second step of SQP optimization, which uses the solution from the first step as an initial guess, can provide a frequency-dependent solution. This process ensures convergence to the global minimum, which leads to the optimum solution. The choice of the number of frequency points depends on the particular structure being investigated. Intuitively, choosing a large number of points always leads to a better solution. However, this is achieved at a higher processing cost. As a rule of thumb, an adequate number of frequency points must be used to properly trace the trajectory of the reflection coefficient in the complex domain.

The measurement setup in Fig. 4 was used to estimate or retrieve ε_r of the individual layers using the cost function F, as expressed in (24) using 11 frequencies within the band. In this experiment, when estimating ε_r of a layer, all of the other parameters (i.e., thicknesses and material properties of other layers) were assumed to be known (consistent with actual practical NDT cases). The results for estimating ε_r of the rubber and acrylic sheets, with and without accounting for the effect of higher order modes, are listed in Table I. These results are compared to the measurements performed using the completely filled waveguide technique [17], [18]. The results indicate that when taking the higher order modes into consideration, the estimated ε_r for the lossy rubber sheet is within less than 1% of the actual ε_r for the real part and within less than 10% for the imaginary part, which is within the accuracy limits of the completely filled waveguide technique [17]. On the other hand, ignoring the higher order modes results in a bias in the estimate of ε_r. This bias is particularly significant when estimating the loss factor. For the low-loss acrylic, ε_r is also accurately estimated when utilizing higher order modes, although the imaginary part is underestimated. This method, like other free-space measurement techniques, is not intended for an accurate measurement of the loss factor of low-loss materials. However, this example shows the improvement in the results when considering the higher order modes. The fact that the real part of ε_r is closely estimated for the acrylic sheet is due the presence of the rubber sheet, which concentrates the radiated fields and significantly reduces the surface waves [19], and hence enhances the measurement. A comparison between the estimated ε_r of the rubber and acrylic shows that when excluding the higher order modes (last column in Table I), the bias in estimating ε_r of the acrylic is not as significant as that for the rubber. This may be attributed to the fact that the acrylic sheet is the second layer in the structure, which makes its contribution to the overall reflection coefficient to be less than the first rubber layer.

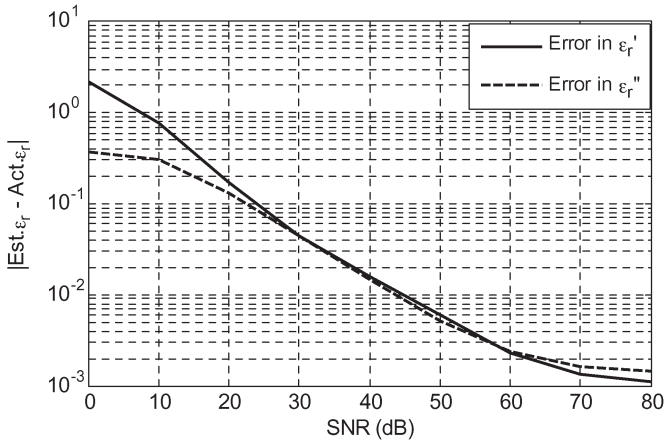

Fig. 5. Complex permittivity estimation error versus SNR.

V. ERROR ANALYSIS

A. Measurement Uncertainty and Noise

As earlier mentioned, all sources of uncertainty may be modeled as a Gaussian-distributed noise (γ) with power of N_o. Fig. 5 shows the average absolute error in estimating the relative complex permittivity of a conductor-backed slab as a function of the signal-to-noise ratio (SNR). These results are semi-empirically obtained through simulating several experiments. In every simulated experiment, an ideal reflection coefficient (e.g., simulated) is contaminated with a Gaussian-distributed noise, as defined by (23), with a certain SNR value. The SNR is defined as

$$\text{SNR} = 10 \log \left(\frac{\frac{1}{N_f} \sum_{i=1}^{N_f} |\Gamma_a(f_i)|^2}{N_0} \right). \tag{25}$$

Subsequently, this contaminated reflection coefficient is used to estimate the relative complex permittivity, as previously described. Two hundred simulations were performed for each

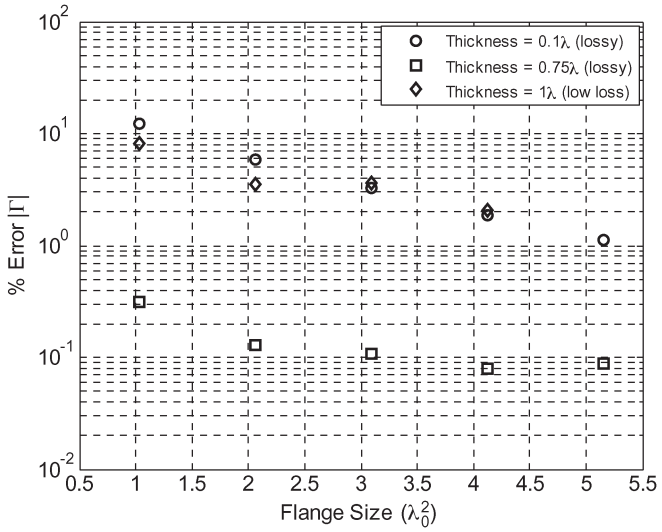

Fig. 6. Effect of flange size on errors in measuring the reflection coefficient for three cases of conductor-backed dielectric slab.

SNR, and the average results are shown in Fig. 5. The results show the performance of this method in estimating the relative complex permittivity of a single conductor-backed layer. Similar simulations may be performed to assess the performance for any given multilayered structure.

B. Effect of Finite Flange

One major source of error in using this method may be due to the finite size of the flange. In previous studies, the flange size was either made very large [10] or chosen based on the pattern of the electric field [11]. Using the electric field pattern method works well in determining the required flange size for a lossy material due to the rapid decay in field strength. However, when the material is thin or low loss, the flange in conjunction with a conductor backing acts as a parallel transmission line that guides the wave toward the edges of the sample, which may cause significant (depending on the desired measurement accuracy) inaccuracies in the measurements due to reflections at the sample edges. To evaluate the effect of flange size, CST-MWS [14] was used to perform 3-D simulations for a conductor-backed single dielectric slab. Cases for various dielectric slab thickness, loss factor, and finite flange sizes were simulated and compared to the case of an infinite flange size (as per Section II). In all of the simulation scenarios, the material and conductor backing were assumed to be infinite in extent. Fig. 6 shows the percent error in measured reflection coefficient versus the flange size for three cases; namely, a thick lossy dielectric slab (0.75λ lossy), a thin lossy slab (0.1λ lossy), and a thick low-loss dielectric slab (1λ low loss). The percent error is defined as

$$\%Error|\Gamma| = 100\frac{1}{N_f}\sum_{i=1}^{N_f}\frac{|\Gamma_{\rm inf}(f_i) - \Gamma_{\rm fin}(f_i)|}{|\Gamma_{\rm inf}(f_i)|} \qquad (26)$$

where $\Gamma_{\rm inf}$ is the measured reflection coefficient using an infinite flange, and $\Gamma_{\rm fin}$ is the reflection coefficient measured using a finite flange. The results show that for a thick lossy material, any flange size larger than (λ_o^2) is sufficient for accurately measuring the reflection coefficient since the error in the reflection coefficient caused by the noninfinite flange is very small ($< 1\%$ equivalent to -40 dB). However, if the dielectric slab is thin or if it is low loss, then a relatively large flange $(> 5\ \lambda_o^2)$ is required to have an accurate measurement of the reflection coefficient. From the results in Figs. 5 and 6, one can design the measurement setup with an adequate flange size to obtain the desired accuracy when estimating the relative complex permittivity. In Fig. 6, the error does not go below 0.1% due to the accuracy of the numerical simulation tool.

VI. Measurements

A. Thin Dielectric Sheets

To verify the effect of slab thickness on estimating the relative complex permittivity, four samples of a lossy rubber with various thicknesses were prepared (Table II). The actual relative complex permittivity of the samples was measured by using the completely filled waveguide technique [18]. Five different cuts of each sample were measured, and the average relative complex permittivities are reported in Table II, as the actual ε_r. Furthermore, these samples showed a very small dispersion of ε_r over the X-band frequencies. The open-ended waveguide measurements were performed with the rubber sheets on a conductor backing. To perform the open-ended waveguide measurements, an X-band waveguide was fitted with a square flange with a side dimension of $5\lambda_o$. Nine measurements were performed on these samples by using an Agilent 8510C VNA and by incorporating 21 frequencies that are equally distributed within the band. A limited number of frequency points are used since the forward model is computationally intensive. On a 2.8-GHz Pentium processor, solving for ε_r at each frequency required 93 s of processing time. First, ε_r was estimated by assuming that the thickness is known, and later, the thickness was estimated assuming that ε_r is known. A summary of the results is shown in Table II. As expected, estimating ε_r of the thin samples, compared to the thicker samples, did not yield accurate results for the loss factor, whereas the real part was estimated with good accuracy. Furthermore, the bias in estimating the loss factor decreased with increasing thickness. Table II also shows that while the thickness is estimated with high accuracy (within 0.1 mm), the effect of ignoring the higher order modes is not significant for this particular case. This may be advantageous since solving for only one mode instead of six modes reduces the processing time by a factor of 16. The insensitivity to the exclusion of higher order modes may be attributed to the fact that the physical thickness is directly proportional to the electrical thickness and hence the real part of ε_r, which is also not significantly affected by the exclusion of higher order modes, as shown in Table I. However, this may not generally be the case, particularly in a multilayered structure with very thin layers in between the thicker layers, where the contribution of the thin layers to the overall reflection coefficient is insignificant.

TABLE II
ESTIMATING THE RELATIVE COMPLEX PERMITTIVITY AND THICKNESS OF VARIOUS RUBBER SAMPLES

Sample #	Actual thickness (mm)	Loaded waveguide technique	Estimated ε_r	Estimated thickness (mm)	
		Actual ε_r		w/ HOM	w/o HOM
Sample 1	0.79	(5.80 ± 0.19) – j (0.34 ± 0.23)	(5.60 ± 0.25) – j (3.32 ± 1.35)	0.80	0.79
Sample 2	3.175	(4.80 ± 0.16) – j (0.17 ± 0.05)	(4.22 ± 0.20) – j (0.43 ± 0.15)	3.13	3.20
Sample 3	6.35	(5.31 ± 0.56) – j (0.22 ± 0.04)	(4.99 ± 0.04) – j (0.21 ± 0.04)	6.39	6.40
Sample 4	12.7	(4.73 ± 0.23) – j (0.24 ± 0.17)	(4.51 ± 0.10) – j (0.14 ± 0.07)	12.24	12.34

TABLE III
ESTIMATING THE THICKNESS OF THIN LAYERS WITHIN A SPECIFIC MULTILAYERED COMPOSITE

Layer #	Material	Relative complex permittivity ε_r	Actual Thickness (mm)	Simulation		Measurement	
				Estimated thickness (mm)		Estimated thickness (mm)	
				w/ HOM	w/o HOM	w/ HOM	w/o HOM
Layer 1	Rubber	4.80 – j 0.17	3.175				
Layer 2	Teflon	2.00 – j 6E-4	0.381	0.385	0.613	0.443	0.632
Layer 3	Rubber	5.31 – j 0.22	6.35				
Layer 4	Teflon	2.00 – j 6E-4	0.508	0.518	0.722	0.616	0.792
Layer 5	Rubber	4.80 – j 0.17	3.175				

B. Thickness Estimation of Thin Disbonds

A particular application for this technique is in the NDT field for estimating the thickness of the thin disbonds and delamination within a multilayered composite structure. Other applications may include measuring the thickness of the adhesive layers in layered composites for quality control purposes. To assess the potential of this technique, a multilayered structure consisting of five layers, as described in Table III, was prepared. Thin Teflon layers were placed in this structure to simulate disbonds and delaminations or adhesive layers in this layered composite. The thickness estimation of the thin Teflon layers was performed by using simulated and measured data. The simulated/measured reflection coefficient was taken with the X-band open-ended waveguide at layer 1 with the structure terminating in an infinite half space of air. The simulated reflection coefficient was obtained by taking 15 modes into consideration, whereas only six modes are used in the estimation process. A random Gaussian noise with a -50-dB variance was added to the simulated reflection coefficient data, as per (23), to mimic the uncertainties due to system noise, calibration errors, and any unwanted reflections. The thicknesses of layers 2 and 4 (representing disbonds) were separately estimated by using 11 frequencies equally spaced in the X-band frequency range. The simulated results show an error of less than 2% when including the higher order modes and an error of up to 60% when excluding the higher order modes. The estimated thicknesses, from the measured reflection coefficient, show an error of about 16% for the thickness of layer 2 and 21% for the thickness of layer 4 when including the higher order modes. The error encountered here may be contributed to the presence of thin air gaps between the layers and the inaccuracies associated with ε_r. The larger error in layer 4 may be due to the farther distance of the layer from the probing open-ended waveguide. On the other hand, excluding the higher order modes resulted in errors of up to 66%.

VII. SUMMARY

The results of formulating the reflection properties of an open-ended rectangular waveguide irradiating a multilayer dielectric composite have been presented. This formulation utilizes Fourier analysis, which provides a complete nonapproximate solution of incorporating any and all of the higher order modes. It has been shown that the contribution of higher order modes is frequency and structure dependent. Most importantly, when measuring the reflection coefficient from a dielectric slab, the effect of the higher order modes significantly increases when the slab is thin relative to the wavelength. A simple analysis was performed to obtain a metric for the performance of this technique in estimating the relative complex permittivity. This analysis was particularly useful in designing the measurement setup given a particular requirement of estimation accuracy. The size of the flange is also an important issue for ensuring an accurate estimation of the loss factor, in particular for thin and low-loss conductor-backed materials. When estimating the relative complex permittivity of the low-loss materials, it may be covered with a lossy slab of dielectric to ensure that no surface wave propagates on the low-loss dielectric, which in turn relaxes the requirement for using a large flange. Furthermore, this technique provides for a better accuracy if the structure is backed with an infinite half space due to the relaxed requirement of flange size. An iterative inverse model (in lieu of a direct inverse approach) was developed with an optimum cost function. This inverse model was used to calculate or retrieve the relative complex permittivity of the thin slabs of rubber and acrylic from measured data. The results showed that when accounting for higher order modes, a significant

improvement in measurement accuracy can be obtained, particularly when there is interest in the retrieving the loss factor. Furthermore, estimating the relative complex permittivity and thickness of several lossy conductor-backed slabs was also demonstrated, highlighting the errors encountered in measuring the loss factor of the thin samples. For this particular case, the thickness estimation was quite robust and was not strongly dependent on the inclusion of higher order modes, which, for this purpose, can be considered to significantly reduce the required processing time. Furthermore, estimating the thickness of a relatively thin and low-loss layer in a multilayered structure was demonstrated using simulated and measured results.

REFERENCES

[1] R. Zoughi, *Microwave Non-Destructive Testing and Evaluation*. Dordrecht, The Netherlands: Kluwer, 2000.

[2] M. A. Abou-Khousa, A. Ryley, S. Kharkovsky, R. Zoughi, D. Daniels, N. Kreitinger, and G. Steffes, "Comparison of X-ray, millimeter wave, shearography and through-transmission ultrasonic methods for inspection of honeycomb composites," in *Proc. Rev. Prog. Quantitative Nondestr. Eval.*, Portland, OR, Jul. 31–Aug. 5, 2006, D. O. Thompson and D. E. Chimenti, Eds. Melville, NY: AIP, 2007, pp. 999–1006, vol. 26B.

[3] M. A. Abou-Khousa and R. Zoughi, "Disbond thickness evaluation employing multiple-frequency near-field microwave measurements," *IEEE Trans. Instrum. Meas.*, vol. 56, no. 4, pp. 1107–1113, Aug. 2007.

[4] J. T. Case, S. Kharkovsky, R. Zoughi, G. Steffes, and F. L. Hepburn, "Millimeter wave holographical inspection of honeycomb composites," in *Proc. Rev. Prog. Quantitative Nondestr. Eval.*, Golden, CO, Jul. 22–27, 2007, D. O. Thompson and D. E. Chimenti, Eds. Melville, NY: AIP, 2008, pp. 970–975, vol. 27B.

[5] S. Bakhtiari, S. Ganchev, N. Qaddoumi, and R. Zoughi, "Microwave non-contact examination of disbond and thickness variation in stratified composite media," *IEEE Trans. Microw. Theory Tech.*, vol. 42, no. 3, pp. 389–395, Mar. 1994.

[6] M. Ravouri, M. A. Abou-Khousa, S. Kharkovsky, R. Zoughi, and R. Austin, "Microwave and millimeter wave near-field methods for evaluation of radome composites," in *Proc. Rev. Quantitative Nondestr. Eval.*, Golden, CO, Jul. 22–27, 2007, D. O. Thompson and D. E. Chimenti, Eds. Melville, NY: AIP, 2008, pp. 976–981, vol. 27B.

[7] V. Theodoris, T. Sphicopoulos, and F. E. Gardiol, "The reflection from an open-ended waveguide terminated by a layered dielectric medium," *IEEE Trans. Microw. Theory Tech.*, vol. 33, no. 5, pp. 359–366, May 1985.

[8] B. A. Sanadiki and M. Mostafavi, "Inversion of inhomogeneous continuously varying dielectric profiles using open-ended waveguides," *IEEE Trans. Antennas Propag.*, vol. 39, no. 2, pp. 158–163, Feb. 1991.

[9] K. Yoshitomi and H. R. Sharobim, "Radiation from a rectangular waveguide with a lossy flange," *IEEE Trans. Antennas Propag.*, vol. 42, no. 10, pp. 1398–1403, Oct. 1994.

[10] C.-W. Chang, K.-U. Chen, and J. Qian, "Nondestructive determination of electromagnetic parameters of dielectric materials at X-band frequencies using a waveguide probe system," *IEEE Trans. Instrum. Meas.*, vol. 46, no. 5, pp. 1084–1092, Oct. 1997.

[11] N. Moade, S. Yong, Y. Jinkui, F. Chenpeng, and X. Deming, "An improved open-ended waveguide measurement technique on parameters ε_r and μ_r of high-loss materials," *IEEE Trans. Instrum. Meas.*, vol. 47, no. 2, pp. 476–481, Apr. 1999.

[12] K. J. Bois, A. D. Benally, and R. Zoughi, "Multimode solution for the reflection properties of an open-ended rectangular waveguide radiating into a dielectric half-space: The forward and inverse problems," *IEEE Trans. Instrum. Meas.*, vol. 48, no. 6, pp. 1131–1140, Dec. 1999.

[13] M. T. Ghasr and R. Zoughi, "Multimodal solution for a rectangular waveguide radiating into a multilayered dielectric structure and its application for dielectric property and thickness evaluation," in *Proc. IEEE IIMTC*, Victoria, BC, Canada, May 12–15, 2008, pp. 552–556.

[14] CST Microwave Studio, *Computer Simulation Technology*, 2008. [Online]. Available: http://www.cst.com/Content/Products/MWS/Overview.aspx

[15] D. L. Faircloth, M. E. Baginski, and S. M. Wentworth, "Complex permittivity and permeability extraction for multilayered samples using S-parameter waveguide measurements," *IEEE Trans. Microw. Theory Tech.*, vol. 54, no. 3, pp. 1201–1209, Mar. 2006.

[16] R. Fletcher, *Practical Methods of Optimization*. New York: Wiley, 1987.

[17] J. Baker-Jarvis, M. D. Janezic, J. H. Grosvenor, and R. G. Geyer, "Transmission/reflection and short-circuit line method for measuring permittivity and permeability," U.S. Dept. Commerce, Boulder, CO, pp. 52–57, Nat. Inst. Sci. Technol. Tech. Note 1355-R, Dec. 1993.

[18] K. Bois, L. Handjojo, A. Benally, K. Mubarak, and R. Zoughi, "Dielectric plug-loaded two-port transmission line measurement technique for dielectric property characterization of granular and liquid materials," *IEEE Trans. Instrum. Meas.*, vol. 48, no. 6, pp. 1141–1148, Dec. 1999.

[19] N. Qaddoumi and R. Zoughi, "Preliminary study of the influences of effective dielectric constant and non-uniform probe aperture field distribution on near-field microwave images," *Mater. Eval.*, vol. 55, no. 10, pp. 1169–1173, Oct. 1997.

M. T. Ghasr (S'01) received the B.S.E.E. degree in 2002 from the American University of Sharjah, Sharjah, United Arab Emerates, and the M.S.E.E. degree in 2004 from the Missouri University of Science and Technology (MST), Rolla, where he is currently working toward the Ph.D. degree.

Since January 2003, he has been with the Applied Microwave Nondestructive Testing Laboratory (AMNTL), MST. His research interests involved developing innovative millimeter-wave imaging techniques, material characterization, and the detection of corrosion and corrosion precursor pitting under paint in aircraft structures using microwave and millimeter-wave nondestructive testing techniques. His current research involves the design and development of a real-time millimeter-wave imaging system.

Devin Simms is currently working toward the B.S.E.E. degree with the Missouri University of Science and Technology (MST) (formerly the University of Missouri-Rolla), Rolla.

Since 2007, he has been an Undergraduate Research Assistant with the Applied Microwave Nondestructive Testing Laboratory (AMNTL), MST. His projects include microwave circuit design and development and material characterization.

Mr. Simms is also an active member of the Gamma Theta chapter of Eta Kappa Nu and the Mo-Beta chapter of Tau Beta Pi.

R. Zoughi (S'85–M'86–SM'93–F'06) received the B.S.E.E, M.S.E.E, and Ph.D. degrees in electrical engineering (radar remote sensing, radar systems, and microwaves) from the University of Kansas, Lawrence.

From 1981 to 1987, he was with the Radar Systems and Remote Sensing Laboratory (RSL), University of Kansas. He was a Professor with the Electrical and Computer Engineering Department, Colorado State University (CSU), Fort Collins, where he established the Applied Microwave Nondestructive Testing Laboratory (AMNTL) and held the position of *Business Challenge Endowed Professor* of electrical and computer engineering from 1995 to 1997. He is currently a *Schlumberger Endowed Professor* of electrical and computer engineering with the Missouri University of Science and Technology (Missouri S&T), formerly University of Missouri-Rolla (UMR), Rolla. He is the author of a textbook entitled *Microwave Nondestructive Testing and Evaluation Principles* (Kluwer, 2000) and the coauthor with A. Bahr and N. Qaddoumi of a chapter on microwave techniques in an undergraduate introductory textbook entitled *Nondestructive Evaluation: Theory, Techniques, and Applications* P. J. Shull, Ed. (Marcel Dekker, 2002). He is the coauthor of over 95 journal papers, 229 conference proceedings and presentations, and 81 technical reports. He has eight patents to his credit, all in the field of microwave nondestructive testing and evaluation.

Dr. Zoughi is a Fellow of the American Society for Nondestructive Testing (ASNT). He is the Editor-in-Chief of the IEEE TRANSACTIONS ON INSTRUMENTATION AND MEASUREMENT. He has been the recipient of numerous teaching awards from both CSU and Missouri S&T.